

Evaluating Uncertainty and Modes of Variability for Antarctic Atmospheric Rivers

1

2 **Christine A. Shields¹, Jonathan D. Wille², Allison B. Marquardt Collow^{3,4}, Michelle**
3 **Maclennan⁵, Irina V. Gorodetskaya⁶**

4 ¹National Center for Atmospheric Research, Climate and Global Dynamics Laboratory, Boulder,
5 Colorado

6 ²Institut des Géosciences de l'Environnement, CNRS/UGA/IRD/G-INP, Saint Martin d'Hères,
7 France

8 ³University of Maryland Baltimore County, Baltimore, MD

9 ⁴Global Modeling and Assimilation Office, NASA Goddard Space Flight Center, Greenbelt, MD

10 ⁵University of Colorado, Department of Atmospheric and Oceanic Science, Boulder, Colorado

11 ⁶CESAM – Centre for Environmental and Marine Studies, Department of Physics, University of
12 Aveiro, Aveiro, Portugal

13

14 Corresponding author: Christine A. Shields (shields@ucar.edu)

15

16

17 **Key Points:**

18

- 19 • Antarctic-specific AR detection tools better capture continental interior footprint
- 20 • Modes of variability (MOVs) generally hold greater influence over West Antarctica than
21 East Antarctica and are consistent across most AR detection tools
- 22 • IOD teleconnections in phase with ENSO produce a stronger AR precipitation response
23 compared to other MOVs

24

25

26 **Abstract**

27 Antarctic atmospheric rivers (ARs) are driven by their synoptic environments and lead to
28 profound and varying impacts along the coastlines and over the continent. The definition and
29 detection of ARs specifically over Antarctica accounts for large uncertainty in AR metrics, and
30 consequently, impacts quantification. We find that Antarctic-specific detection tools consistently
31 capture the AR footprint inland over the ice sheets, whereas most global detection tools do not.
32 Large-scale synoptic environments and associated ARs, however, are broadly consistent across
33 detection tools. Using data from the Atmospheric River Tracking Method Intercomparison
34 Project and global reanalyses, we quantify the uncertainty in Antarctic AR metrics as well as
35 evaluate large-scale environments in the context of decadal and interannual modes of variability.
36 The Antarctic western hemisphere has stronger connections to both decadal and interannual
37 modes of variability compared to East Antarctica, and the Indian Ocean Dipole (IOD)'s
38 influence on Antarctic ARs is stronger while in phase with ENSO.

39

40 **Plain Language Summary**

41 Atmospheric rivers (ARs) are large-scale weather features that transport significant amounts of
42 moisture and are akin to “rivers in the sky”. ARs traveling to Antarctica from the mid-latitudes
43 can bring enough moisture to produce extreme snowfall, or if accompanied by warm air, can
44 result in melt events, both of which affect ice sheets across the continent. How we define ARs in
45 gridded datasets significantly impact what we say about them. If a definition uses Antarctic-
46 specific constraints, it does a better job at describing the actual spatial footprint for ARs
47 impacting inland locales on the continent. The large-scale environments that produce ARs, and
48 how these environments naturally vary, however, are generally consistent regardless of how we

49 define ARs. ARs impacting the western hemisphere of Antarctica are more deeply connected to
50 specific atmospheric patterns that repeatedly occur compared to weaker connections with East
51 Antarctic ARs.

52

53

54

55

56

57

58

59

60

61

62

63

64

65

66

67 **1 Introduction**

68 Atmospheric rivers (ARs) are long, narrow synoptic-scale weather phenomena that serve as
69 meridional transport vehicles important for both large-scale and local hydrological climate across
70 the globe. ARs transport both water and energy from lower to high latitudes and are often
71 connected to extratropical cyclones where moisture laden bands of water vapor and clouds
72 extend and travel across and along baroclinic zones (Ralph et al., 2018, AMS Glossary of
73 Meteorology, 2017). Although the bulk of the current literature describe ARs in mid-latitude
74 locations impacting western coasts of continents, such as western North America and western
75 Europe, ARs are equally important in polar regions where the interaction of these moisture
76 streams with land and sea ice, result in consequential precipitation events impacting the local
77 cryosphere (Turner et al., 2019, Mattingly et al., 2018). Specific to Antarctica and depending on
78 the thermal characteristics, ARs can produce significant snow accumulation over the ice sheet,
79 (Gorodetskaya et al., 2014, Adusumilli et al., 2021, Terpstra et al., 2021, Wille et al., 2021), or
80 melt events with consequences for ice shelf stability (Wille et al., 2019, Wille et al., 2022, Turner
81 et al., 2022, Clem et al., 2022). Generally, ARs reaching Antarctica are relatively rare
82 occurrences (Wille et al., 2021), fully extending into the continent only a few times per year but
83 clearly tied to favorable synoptic conditions, such as blocking events in the Southern Ocean that
84 funnel ARs into the continent (Wille et al., 2021, Pohl et al., 2021, MacLennan et al., 2021,
85 Bozkurt et al., 2018, Terpstra et al., 2021). Despite their low frequency, they account for the
86 largest percentage of total precipitation observed over Antarctica (Turner et al. 2019, Wille et al.,
87 2021) and have important consequences for the continent's hydroclimate. ARs can also be tied
88 to teleconnections and modes of natural variability (MOVs). AR occurrences for different
89 regions around Antarctica have been attributed to various MOVs, such as the Southern Annular

90 Mode (SAM) (Wille et al., 2021, Clem et al., 2016, Raphael et al., 2016, Marshall et al., 2016),
91 the Pacific South American Mode 2 (PSA2) (MacLennan et al., 2021, Marshall et al., 2016), the
92 Pacific Decadal Oscillation (PDO) (Turner et al., 2019, Fogt et al., 2019), the Indian Ocean
93 Dipole and El Nino Southern Oscillation (IOD, ENSO, respectively) (Nuncio and Yuan, 2015).
94 Parts of the cold temperature anomalies in West Antarctica can also be explained by the
95 influence of the Indian Ocean Basin mode and Atlantic Zonal and Meridional Modes (Li et al.,
96 2015; Lee and Jin, 2021; Gutierrez et al., 2021, Table Atlas.1). In this study, we explicitly
97 evaluate the relationship between these MOVs, ARs, and their associated precipitation and
98 boundary layer temperature, to characterize the varied impacts across different regions and
99 flavors of ARs. We do not evaluate surface impacts themselves, such as surface mass balance on
100 glaciers, rather, we focus on understanding the large-scale variability that drives these impacts.
101 Although we do not consider here an exhaustive list of MOVs of consequence for ARs, we limit
102 this study to the decadal and interannual bimodal indices of variability introduced above.
103 Additionally, because the very definition an AR is often debated (i.e., is the feature simply a
104 moisture transport alone, or rather, connected to an extratropical cyclone) (Shields et al., 2019,
105 Ralph et al., 2018, Gimeno et al., 2021) we quantify the uncertainties in AR metrics such as
106 occurrence and climatology, as well as MOV impact, to provide context for our results.

107

108 **2 Data and Methods**

109 **2.1 Reanalysis Datasets**

110 We employ both the Modern Era Retrospective Analysis for Research and Applications, version
111 2 (MERRA-2) (Gelaro et al., 2017) and European Centre for Medium-Range Weather Forecasts'

112 Reanalysis Version 5 (ERA5) (Hersbach et al., 2020) global reanalyses in this work. To
113 represent large scale synoptics and analyze modes of variability, we primarily use MERRA-2,
114 which explicitly represents the energy and hydrologic budgets over ice sheets in Antarctica
115 (Gelaro et al., 2017). A more in-depth evaluation of the cryosphere in MERRA-2 is available in
116 Section 9 of Bosilovich et al. (2015) as well as Gossart et al. (2019). Sea surface temperature and
117 sea ice concentration in MERRA-2 are prescribed as indicated by Table 3 of Gelaro et al. (2017).
118 At approximately 50 km resolution, MERRA-2 is sufficient to resolve weather features, such as
119 atmospheric rivers, along with their associated precipitation, and is the baseline dataset for the
120 Atmospheric River Tracking Method Intercomparison Project (ARTMIP) (Shields et al., 2018,
121 Rutz et al., 2019). ARTMIP provides a collection of AR “catalogues” from a variety of ARDTs
122 (Atmospheric River Detection Tools) that detail gridded and timeslice information on where and
123 when ARs exist. Using MERRA-2 across the same years as included in ARTMIP (1980-2016)
124 allows us to consistently apply all available ARTMIP ARDT catalogues to Antarctic AR
125 uncertainty quantification. ERA5 datasets are also applied (1980-2020), where available, to
126 further represent the spread in climatology metrics across both ARDT and reanalysis products
127 and robustly quantify uncertainty by using as many catalogues as possible. Monthly MERRA-2
128 data is used to compute MOV indices (GMAO, 2015a; GMAO, 2015b), daily data to compute
129 precipitation (GMAO, 2015c) and 850 hPa temperature (GMAO, 2015d) for AR days, and 3-
130 hourly data is used for AR identification (GMAO, 2015d). Only ARDTs with polar constraints
131 (those that incorporate a lower threshold designed for polar latitudes, here referred to as P-
132 ARTMIP) are used for MOV analysis to minimize errors by only including appropriately
133 designed ARDTs.

135 **2.2. Atmospheric River Detection**

136 Identification and tracking of ARs require decisions dependent on the AR definition. Because
137 this definition varies wildly from one project to another (Ralph et al., 2018, Rutz et al., 2019),
138 metrics such as AR frequency and seasonality differ depending on choice of ARDT. ARTMIP
139 has shown that uncertainty based on ARDT far outweighs uncertainty based on model (O'Brien
140 et al., 2021) as well as reanalysis (Collow et al., 2022). Thus, uncertainty quantification is an
141 important component to any analysis where AR detection is required. It is also important to
142 recognize that applying many different ARDTs for each science problem is not always practical
143 for individual researchers, so a balance must be struck to address ARDT uncertainty, either by
144 applying multiple ARDTs, such as this work and ARTMIP, or minimally, determining if the
145 chosen ARDT is fit for purpose (Rutz et al., 2019). Traditional ARDTs designed for the mid-
146 latitudes typically apply moisture thresholds using the quantity called integrated vapor transport
147 (IVT). However, for ARs making landfall and extending poleward onto the continent, one option
148 is to identify ARs by simply using the meridional component. Here, we primarily apply
149 Antarctic-specific ARDTs to diagnose the relationship between MOVs and ARs across
150 Antarctica but include all methods with polar constraints to represent uncertainty spread. For
151 climatology metrics, we include all available global ARTMIP ARDTs to highlight the large
152 differences in metrics. The Antarctic-specific algorithms, herein referred to as Wille_vIVT and
153 Wille_IWV, focus on meridional geometry and filter for high (98% percentile) relative moisture
154 flow into the continent to better capture ARs impacting polar latitudes, rather than zonally
155 around the Southern Ocean. Further details on Wille the ARDTs (Wille et al., 2019, Wille et al.,
156 2021), ARTMIP ARDTs, and IVT/IWV calculations are in Supplemental.

157

158 **2.3 Modes of Variability**

159 We calculate both decadal and interannual modes of variability consistent with the Climate
160 Variability and Diagnostic Package (CVDP) developed by Phillips et al., 2014. Modes were
161 chosen based on current literature, as described in the introduction, with an already established or
162 potential connection to AR impacts in and around Antarctica. Decadal modes are represented
163 here by the SAM and the PDO, and for interannual modes, PSA2 and IOD, both in and out of
164 phase with ENSO. All of these indices have been found to influence both Antarctic precipitation
165 and temperature (as summarized in Gutierrez et al., 2021, Table Atlas 1). Specific details on
166 computation are found in supplemental material. One caveat to using the PDO is the relatively
167 short timespan of available data of ~four decades. Tropical pacific decadal variability (TPDV)
168 such as the PDO have timescales from 8 to 40 years (Power et al., 2021), making significance
169 testing challenging. Because we are limited to the ARTMIP time period and thus only 37 years
170 are used, PDO and AR correlations are shown for qualitative illustration, but significance
171 inferences are limited and used with caution.

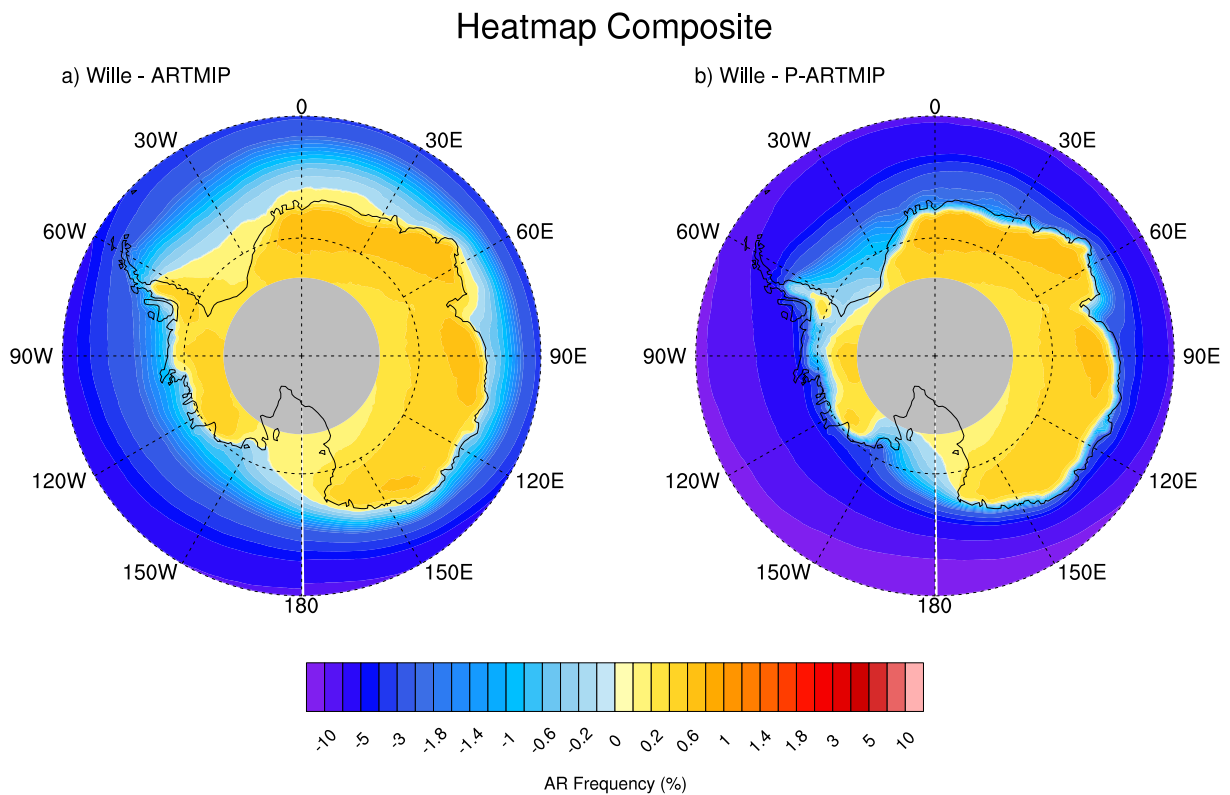
172

173 **3 Climatological characteristics and uncertainty due to ARDT**

174 ARs impacting high latitude locales such as Antarctica do not necessarily follow mid-latitude
175 storm tracks. Rather, ARs often bend and flow around high-pressure blocks or follow baroclinic
176 zones connected to low pressure regimes ultimately pushing moisture intrusions into the
177 continent. ARs that make it onto the continent are dominated by the north-south meridional
178 component of the wind (not shown). This can be demonstrated by computing heat maps of AR
179 occurrence for each method and comparing the Antarctic specific occurrences to traditional
180 methods developed for mid-latitudes. Figure 1a shows the spatial distribution differences

181 between the mean Wille Antarctic-specific ARDTs and the ARTMIP mean. ARs that make
 182 landfall are generally rare (a few times per year, Wille et al., 2021), but even so, the Antarctic
 183 specific ARDTs consistently detect ARs in the interior of the continent where most traditional
 184 ARDTs detect more in the Southern Ocean. Even global ARDTs that allow for polar thresholds
 185 (P-ARTMIP) (Figure 1b) ultimately do not capture ARs on the interior ice sheets, especially over
 186 East Antarctica. This is likely because the Antarctic specific ARDTs applied here focus on the
 187 meridional component of the moisture transport that allows for AR detection deeper into the dry
 188 Antarctic interior.

189



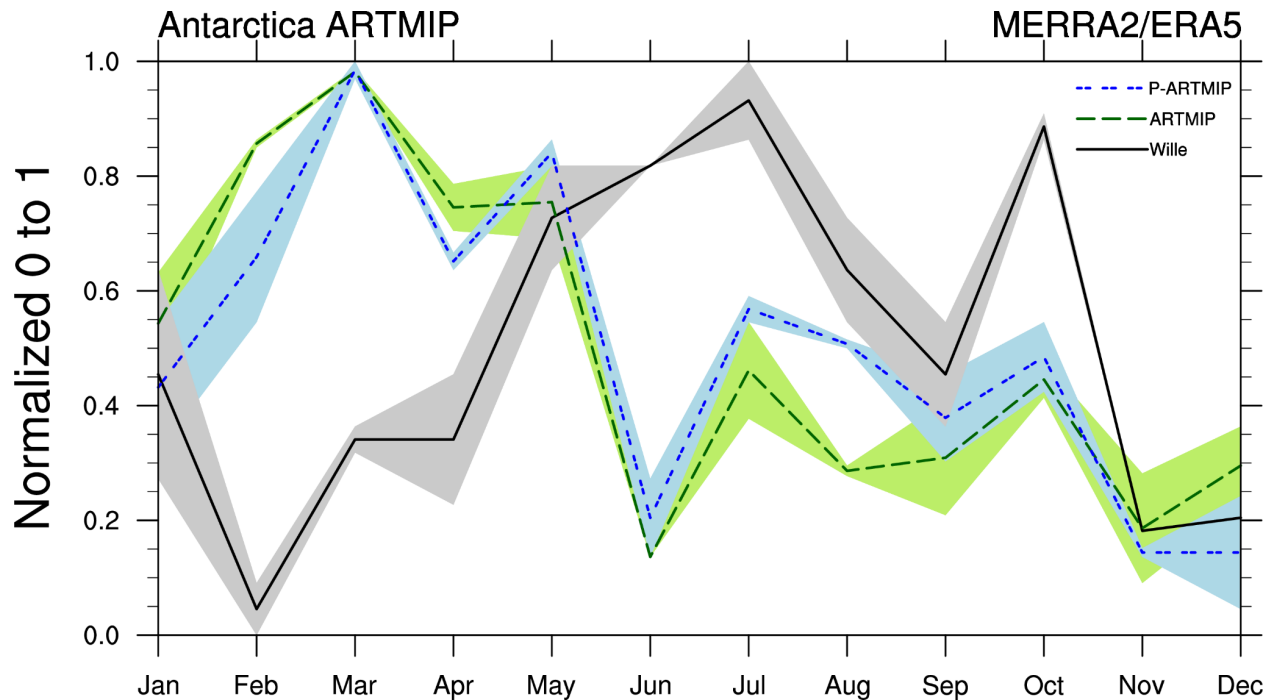
190

191

192 **Figure 1.** Composite difference heatmaps of AR frequency in % time (relative to the entire
193 ARTMIP MERRA-2 timespan, 1980-2016). Wille ARDTs versus all applicable global ARDTs
194 (a) and Wille ARDTs versus P-ARTMIP (b).

195

196 From a continent-wide, climatological perspective, (Figure 2), the Wille ARDTs detect ARs
197 distributed throughout the year, with maximum occurrence in Austral fall and winter, consistent
198 with instrumental observations and Regional Climate Model (RACMO2) that show high
199 accumulation events with synoptic conditions for both West Antarctica over Thwaites Glacier
200 ($\sim 108.5^\circ\text{W}$) (MacLennan et al., 2021, Lenaerts, et al., 2018) and East Antarctica over Dronning
201 Maud Land ($\sim 20^\circ\text{W} - 45^\circ\text{E}$) (Gorodetskaya et al., 2014). (See Figure S1 in supplemental for
202 Antarctic geography). Distinctly different from Wille ARDTs, ARs detected from global and P-
203 ARTMIP methods, peak in February and Austral Fall, and are likely due to the predominance of
204 ARs impacting the Antarctic Peninsula, which in some cases, are the only location where ARs
205 are identified (Supplemental Figures 3 and 4). Because of the geographic position of the
206 Peninsula in the Southern Ocean, the global ARDTs, designed for mid-latitudes, capture more
207 zonally-oriented ARs. Specific regional climatologies (Antarctic Peninsula, Dronning Maud
208 Land, and Princess Elizabeth/Queen Mary Lands, $\sim 73^\circ\text{E}-100^\circ\text{E}$) can be found in Supplemental.
209



210

211

212 Figure 2. Antarctic seasonal cycle of ARs for ARTMIP mean (lines) and spread (shading) which
 213 includes applicable available ARDTs (Supplemental Table S1, Figure S3) and both reanalysis
 214 datasets ARTMIP Tier 1 MERRA-2 and Tier 2 ERA5. All available global ARDTs (ARTMIP)
 215 versus ARTMIP with polar constraints (P-ARTMIP) versus Antarctic specific (Wille ARDTs).

216

217 4 Relationship between Antarctic ARs and MOVs

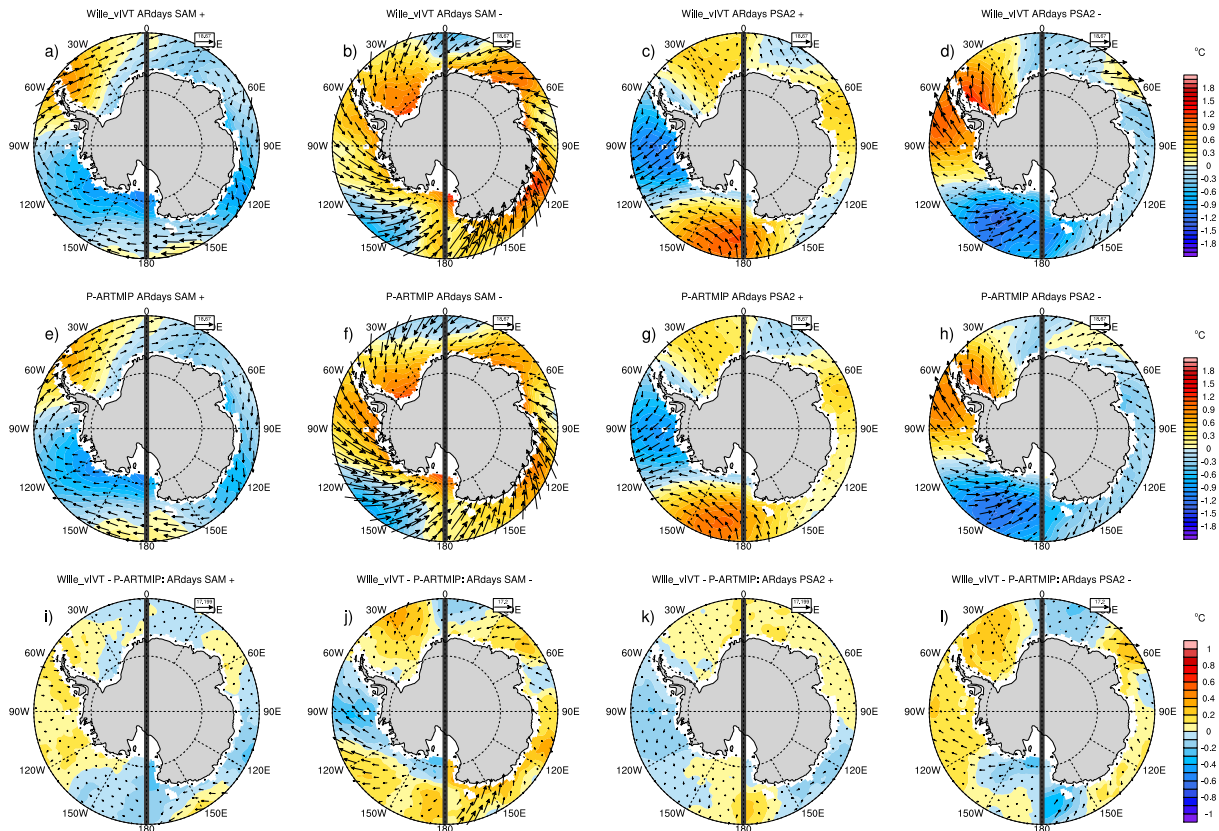
218 4.1 MOV Synoptics for AR days

219 Around and across Antarctica, there are a variety of different climate regimes, but coastal
 220 climates depend on geometry and orientation of the coast relative to the zonal and meridional
 221 flow. However, for the purposes of evaluating broad synoptic influences, we divide our study
 222 into West and East Antarctica. To isolate and amplify unique west and east hemispheric patterns,
 223 we apply the split hemisphere technique, commonly used for peak (seasonal) tropical cyclone

224 track density analysis (Korty et al., 2012, Yan et al., 2016), except here, we composite synoptic
225 conditions for landfalling ARs for each, respective hemisphere. That is, for days where ARs
226 impact West Antarctica, synoptic conditions are composited for the western hemisphere, and for
227 days where ARs impact East Antarctica, synoptic conditions are composited for the eastern
228 hemisphere. All spatial figures presented here contain a solid thick line dividing as a reminder
229 that the hemispheres are treated separately but plotted together for illustration. We highlight the
230 Wille_vIVT ARDT because this algorithm better represents AR dynamics (Wille et al., 2021).
231 Figure 3 plots annual anomalies for low-level (850 hPa) moisture flux (vectors) and temperature
232 (contours) for AR days occurring during the different phases of SAM and PSA, a decadal and
233 interannual mode of variability, respectively, that represents variations in the dynamics. Across
234 polar ARDTS (Fig. 3 e-h), clearly show the fluxes in (SAM positive Antarctic Peninsula, PSA2
235 negative for the West Antarctic Ice Sheet, Amundsen and Ross Seas (Figure S1) and out of the
236 continent for the western hemisphere, consistent with Antarctic MOV patterns in Marshall and
237 Thompson (2016) and Marshall et al. (2017). For East Antarctica, the fluxes are varied but
238 generally the opposite, with, for example, Dronning Maud Land showing fluxes into the
239 continent during SAM negative. Overall PSA2 holds greater influence for the western
240 hemisphere, and results are consistent across all global ARDTs, regardless of polar constraints or
241 not (not shown). Across ARDTs for AR days, although there are variations in boundary layer
242 temperature, moisture, and winds, synoptic conditions are robust across methods, unlike
243 frequency metrics and seasonal climatology although some regional differences exist from
244 Wille_vIVT (Fig 3 i-l), our primary method. For example, SAM-, the Wille_vIVT ARDT detects
245 more ARs with onshore flow (~180-150°E) to Terre Adelie Land (~140 E) (Fig 3j).

246

247



248

249 Figure 3. Anomalies of 850 hPa Air temperature for AR day composites (color contours, °C) and
 250 850 hPa moisture flux ($\text{kg m}^{-1}\text{s}^{-1}$)(arrows) during SAM phases (a-b,e-f,i-j), PSA2 phases (c-d,g-
 251 h,k-l) in split hemisphere format. West Antarctic ARs are composited separately from East
 252 Antarctic ARs to maintain unique hemispheric synoptic signatures and combined for illustration,
 253 separated by thick gray line. Wille_vIVT (a-d), ARTMIP mean for ARDTs with polar
 254 constraints (P-ARTMIP) (e-h) and differences (i-l) are shown. Reference vector is shown in the
 255 box at the upper right of each panel.

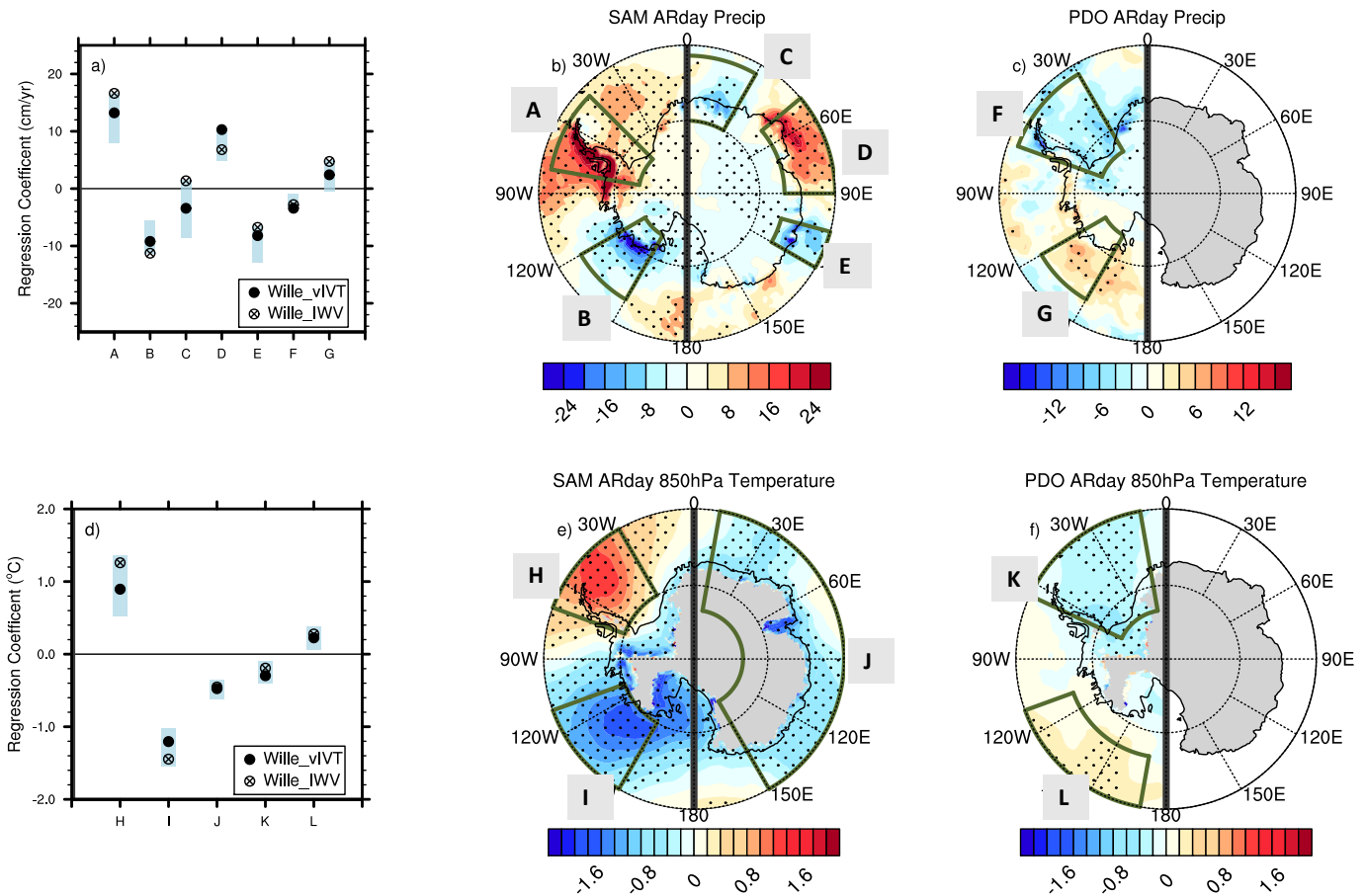
256

257 4.2 Precipitation and temperature impacts

258 4.2.1 Decadal modes of variability: SAM and PDO

259 Decadal modes of variability, their relationship with AR precipitation and 850 hPa temperature, and
260 ARTMIP uncertainty, is shown in Figure 4. Again, we highlight the Wille_vIVT ARDT for spatial plots
261 that regress PC timeseries for SAM (Fig. 4b, e) and PDO (Fig. 4c, f) onto precipitation and temperature
262 anomalies for AR days. For the PDO, we show western hemisphere only due to the lack of any
263 significance elsewhere. Both precipitation and temperature follow the composite plots for AR days (Fig.
264 3) in that where moisture fluxes flow into the continent, enhanced precipitation occurs, along with
265 corresponding temperature anomalies. For example, SAM in the positive phase typically indicates a
266 deeper Amundsen Sea Low (and vice-versa), and generally less mass transport between Antarctica and
267 the southern mid-latitudes (Turner et al., 2013, Spensberger et al., 2020). Figure 4b shows the
268 precipitation is positively and significantly correlated with SAM over Antarctic Peninsula (label A) and
269 negatively correlated over the Amundsen sea region (label B), resulting from a deeper Amundsen Sea
270 Low that brings cyclonic, clockwise flow into the Peninsula and out of the Amundsen sea region during
271 SAM positive. SAM negative, oppositely correlated with precipitation between Amundsen and Ross
272 Seas near Marie Byrd Land ($\sim 120^\circ\text{W}$), supports onshore flow during the negative phase. The eastern
273 hemisphere shows less significance in precipitation although SAM's influence is hinted at in regions
274 such as Dronning Maud Land, Kemp Land and the Amery Ice Shelf, and Wilkes Land (labels C, D, E,
275 respectively; supplemental Figure S1 for Antarctic locations). The PDO shows a negative correlation
276 with the Antarctic Peninsula in both temperature and precipitation (labels K, F), and a positive one
277 between the Amundsen and Ross Seas (labels L, G), although significance is weak and overall shows
278 less influence than SAM. Each region that shows significance is tested across all P-ARTMIP algorithms
279 (Fig. 4a, d) to quantify uncertainty in these calculations. Across most regions and methods, the sign of
280 the correlation is robust for both temperature and precipitation, except for Dronning Maud Land (DML)

281 for precipitation (label C), where the strength of the correlation is generally tied to frequency
 282 climatology.



283
 284
 285 Figure 4. Regression patterns and spread for AR days and decadal modes of variability (SAM
 286 and PDO). Precipitation (cm yr^{-1}) (b-c) and 850 hPa temperature ($^{\circ}\text{C}$) (e-f) patterns are plotted
 287 for Wille_vIVT ARDT. Uncertainty is shown for area-averaged regression values across all P-
 288 ARTMIP ARDTs (a,d). Dark green boxes indicate areas used in the uncertainty calculation and
 289 are labeled alphabetically. Split hemisphere format, as Figure 3, is used. The PDO is shown for
 290 western hemisphere only. Significance was tested at 90% level using a student T-test. Where

291 shown, 850 hPa temperatures are plotted for topographical regions under 850 hPa highlighting
292 coastal and escarpment zones and eliminating errors on pressure surfaces due to elevation.

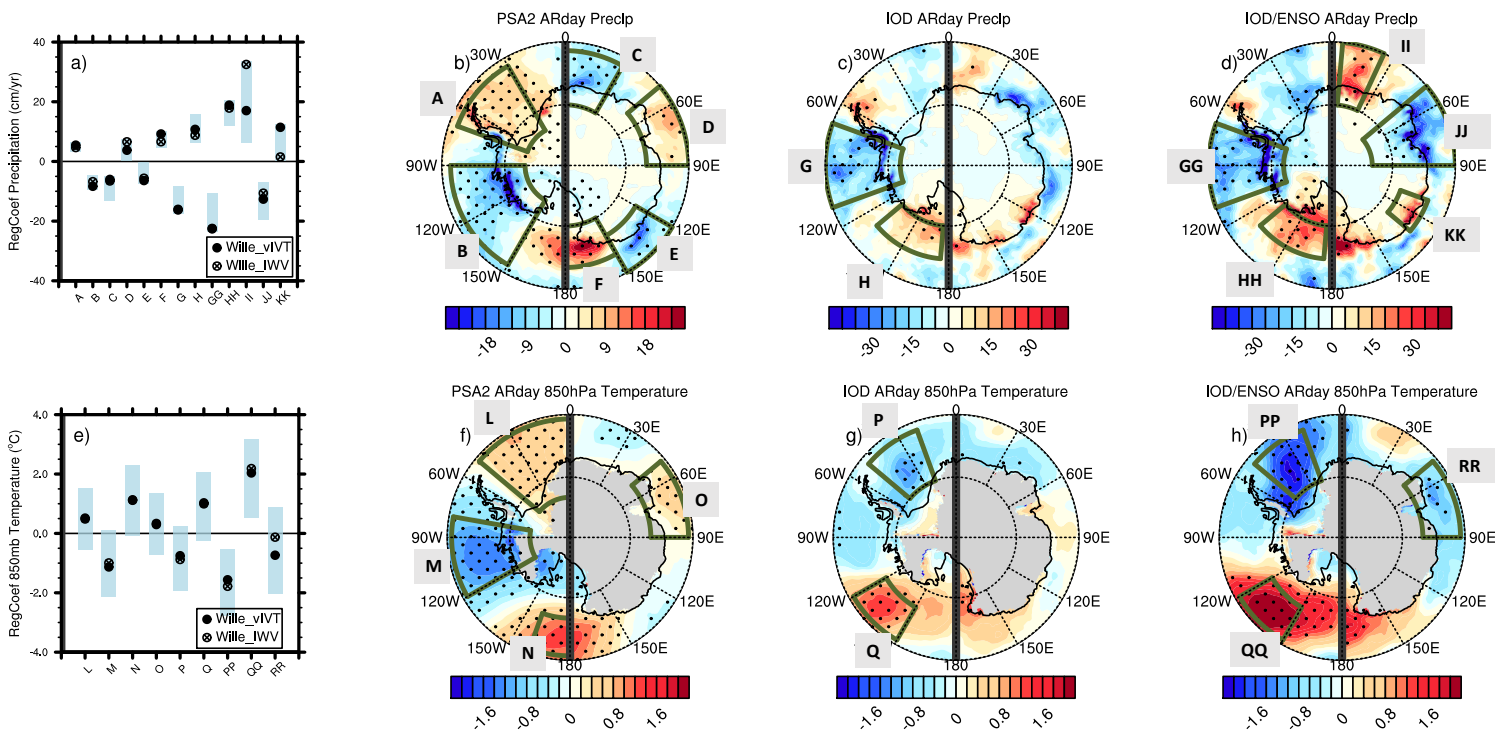
293

294 **4.2.2 Interannual modes of variability: PSA2, IOD and ENSO**

295 Interannual modes of variability, their relationship with AR precipitation and 850 hPa temperature, and
296 ARTMIP uncertainty, is shown in Figure 5. We evaluate PSA2 and IOD independently to illustrate their
297 dominant, spatial impacts. However, it is important to note that no MOV, and especially interannual
298 modes, operate in isolation. The PSA2 mode has been shown to excite sea surface temperature (SST)
299 patterns tied to the evolution of ENSO (Lou et al., 2021), and the IOD is often paired with ENSO, in
300 addition to decadal modes such as PDO. For simplicity, we evaluate the dynamical mode of PSA2
301 separately from modes defined by SST anomalies (IOD, ENSO). The PSA2 has already been shown to
302 have significant implications for the Amundsen Sea Embayment and Thwaites Glacier (MacLennan et
303 al., 2021), and we confirm this with our regression analysis that shows negative correlation with PSA2
304 and precipitation in this area (label B), consistent with flux composites in Figure 3 and a potential
305 amplification of wavenumber 3 (Cai et al., 1999). Temperature anomalies for AR days also align with
306 regressions where poleward flow from mid-latitudes brings warmth into the Ross Sea region and is
307 positively correlated with PSA2 (label N) compared to equatorward flow, negative correlations, and
308 colder temperature over Amundsen Sea (label M). The IOD (Fig 5c-d, g-h) is much more potent while
309 in phase with ENSO with negative correlations over West Antarctic regions such as Ellsworth Land
310 (labels GG, PP) and positive correlations with Eastern Dronning Maud Land (label II) and Ross Sea
311 (labels HH, QQ). Temperature significance is stronger than precipitation significance, however, likely
312 tied to the broad extratropical SST influences during these modes. Although significance with
313 Wille_vIVT is strong for temperatures, the differences with Wille_IWV and the P-ARTMIP spread

314 (Fig5 a, e) suggest this result is not necessarily robust across ARDTs, and even potentially changes the
 315 sign of the correlation. Precipitation uncertainty is smaller, with most of the methods agreeing on
 316 correlation signs except for the IOD responses near Wilkes Land (label KK). Finally, the amplitude of
 317 IOD-ENSO response is much higher than any other MOV, interannual or decadal, suggesting that the
 318 IOD in phase with ENSO produces more anomalous precipitation than any other mode studied here.
 319 Nuncio and Yuan (2015) describe Antarctic sea ice correlations during IOD with ENSO in the Pacific
 320 sector and Ross Seas, and note the decrease is sea ice corresponding to warm meridional flow.
 321 Additionally, the wave train schematic in Nuncio and Yuan (2015) is consistent with our results that
 322 show for AR days, precipitation and warm low-level temperatures are positively correlated due to
 323 enhanced poleward flow at the Ross Sea and equatorward flow off the West Antarctic Ice Sheet.

324



326

327 Figure 5. Same as Fig 4 except for interannual modes of variability PSA2 (b,f), IOD without (c,g)
328 and IOD in phase with ENSO (d,h). Significance was tested at 90% level using a student T-test. Note
329 precipitation contour scales are different for PSA2 versus IOD.

330

331 **5 Conclusions**

332 Studying Antarctic atmospheric rivers combines a unique set of disciplines incorporating both
333 atmospheric science and the cryosphere, but also cross-disciplinary interests such as feature
334 detection. To understand this phenomenon, we must both define it and put it into context with
335 current research. Antarctic AR detection tools are generally robust across the synoptic
336 meteorology, however large uncertainties exist for AR frequency climatology metrics such as
337 seasonal cycle and location of landfall. Antarctic-specific tools that rely on the meridional
338 characteristics of ARs capture the continental interior footprint of ARs more consistently
339 compared to global ARDTs designed for the mid-latitudes. When evaluating ARs in the context
340 of modes of natural variability (SAM, PSA2, PDO, IOD and ENSO), this study finds the MOVs
341 studied here influence West Antarctic ARs more than East Antarctica. Spread among ARDTs is
342 generally smaller for decadal modes of variability compared to interannual modes. This is likely
343 due to the shorter period for interannual modes and the opportunity for compounding MOV
344 events. Additionally, the Indian-ocean dipole teleconnections with ENSO produce a stronger AR
345 response, mostly for West Antarctica and the Pacific sector, compared to other MOVs. Although
346 we have chosen to diagnose MOVs that sample both decadal and interannual variability, it is not
347 a complete list of potential influences on ARs onto the Antarctic glaciers and ice shelves. Future
348 work includes understanding compound MOVs beyond IOD and ENSO. With our exploration of
349 IOD and ENSO, compound MOVs clearly have the potential to amplify or suppress AR activity.

350 Understanding the interplay between MOVs and ARs improves predictability and the ability to
351 manage consequences as we move into a warmer climate. A future increase in MOVs that favor
352 AR landfalls and warmer conditions will likely increase snowfall in the impacted area, but also
353 risk increased surface melt and ice shelf destabilization.

354

355 **Acknowledgments**

356 This work is supported by the U.S. Department of Energy, Office of Science, Office of
357 Biological & Environmental Research (BER), Regional and Global Model Analysis (RGMA)
358 component of the Earth and Environmental System Modeling Program under Award Number
359 DE-SC0022070 and National Science Foundation (NSF) IA 1947282 and by the National Center
360 for Atmospheric Research (NCAR), sponsored by the NSF Cooperative Agreement No.
361 1852977. ARTMIP is a grass-roots community effort. Details on ARDTs can be found on the
362 ARTMIP website, <https://www.cgd.ucar.edu/projects/artmip/algorithms.html>, but we specifically
363 thank B. Guan, J. Lora, M. Krinisky, K. Kashinath, E. McClenny, K. Nardi, M. Pan, K. Reid, J.
364 Rutz, T. O'Brien, E. Shearer, P. Ullrich, G. Xu) for their catalogues. ARTMIP DOE (BER)
365 RGMA and the Center for Western Weather and Water Extremes (CW3E) at Scripps Institute for
366 Oceanography at the University of California, San Diego. J. D. W. acknowledges support from
367 the Agence Nationale de la Recherche project, ANR-20-CE01-0013 (ARCA). M. L. Maclennan
368 acknowledges support from NASA FINESST grant 80NSSC21K1610.

369 **Open Research**

370 ARTMIP data is available from the Climate Data Gateway <https://doi.org/10.5065/D6R78D1M>
371 and <http://doi.org/10.5065/D62R3QFS>. MERRA-2 is available from the Goddard Earth Sciences

372 Data and Information Services Center (GES DISC) at <https://disc.gsfc.nasa.gov/>, DOI numbers
373 doi: 10.5067/9SC1VNTWGWV3 and doi: 10.5067/Q5GVUVUIVGO7. ERA5 data is available
374 from the Copernicus Climate Change Service (C3S) Climate Data Store at
375 <https://cds.climate.copernicus.eu/cdsapp#!/dataset/reanalysis-era5-single-levels?tab=overview>.

376 **References**

377 Adusumilli, Susheel, Meredith A Fish, Helen Amanda Fricker, and Brooke Medley. (2021),
378 Atmospheric river precipitation contributed to rapid increases in surface height of the west
379 Antarctic ice sheet in 2019, *Geophysical Research Letters* 48, no. 5: e2020GL091076.

380

381 American Meteorological Society, (2017). Atmospheric river. Glossary of Meteorology,
382 http://glossary.ametsoc.org/wiki/Atmospheric_river.

383

384 Bosilovich, M. G., and Coauthors, (2015). MERRA-2: Initial evaluation of the climate.
385 *Technical Report Series on Global Modeling and Data Assimilation*, Vol. 43, NASA Tech. Rep.
386 NASA/TM–2015–104606, 139 pp. [Available online at
387 <https://gmao.gsfc.nasa.gov/pubs/docs/Bosilovich803.pdf>.]

388

389 Bozkurt, D., Rondanelli, R., Marin, J. C., & Garreaud, R. (2018). Foehn event triggered by an
390 atmospheric river underlies record-setting temperature along continental Antarctica. *Journal of*
391 *Geophysical Research: Atmospheres*, 123, 3871– 3892. [https://doi-](https://doi-org.cuucar.idm.oclc.org/10.1002/2017JD027796)
392 [org.cuucar.idm.oclc.org/10.1002/2017JD027796](https://doi-org.cuucar.idm.oclc.org/10.1002/2017JD027796)

393 Cai, W., Baines, P. G., & Gordon, H. B. (1999). Southern Mid- to High-Latitude Variability, a
394 Zonal Wavenumber-3 Pattern, and the Antarctic Circumpolar Wave in the CSIRO Coupled
395 Model, *Journal of Climate*, 12(10), 3087-3104.

396 Clem, K. R., Renwick, J. A., McGregor, J., and Fogt, R. L. (2016), The relative influence of
397 ENSO and SAM on Antarctic Peninsula climate, *J. Geophys. Res. Atmos.*, 121, 9324– 9341,
398 doi:10.1002/2016JD025305.

399 Clem, K.R., Bozkurt, D., Kennett, D., King, J., Turner, J. (2021). Central tropical Pacific
400 convection drives extreme high temperatures and surface melt on the Larsen ice shelf, 11 August
401 2021, PREPRINT (Version 1) available at Research Square [[https://doi.org/10.21203/rs-
402 712751/v1](https://doi.org/10.21203/rs.3.rs-712751/v1)]

403

404 Collow, A. B. M., Shields, C. A., Guan, B., Kim, S., Lora, J. M., McClenny, E. E., et al. (2022).
405 An overview of ARTMIP's Tier 2 Reanalysis Intercomparison: Uncertainty in the detection of
406 atmospheric rivers and their associated precipitation. *Journal of Geophysical Research:
407 Atmospheres*, 127, e2021JD036155, <https://doi.org/10.1029/2021JD036155>.

408

409 Francis, D., Mattingly, K. S., Temimi, M., Massom, R., & Heil, P. (2020). On the crucial role of
410 atmospheric rivers in the two major Weddell Polynya events in 1973 and 2017 in Antarctica.
411 *Science Advances*, 6(46), eabc2695.

412

413 Fogt, R.L. and Clem, K.R., (2020). Connections with middle and low latitudes. *In Past*
414 *Antarctica* (pp. 219-239). Academic Press.

415

416 Gelaro, R., McCarty, W., Suárez, M. J., Todling, R., Molod, A., Takacs, L., Randles, C. A.,
417 Darmenov, A., Bosilovich, M. G., Reichle, R., Wargan, K., Coy, L., Cullather, R., Draper, C.,
418 Akella, S., Buchard, V., Conaty, A., da Silva, A. M., Gu, W., Kim, G., Koster, R., Lucchesi, R.,
419 Merkova, D., Nielsen, J. E., Partyka, G., Pawson, S., Putman, W., Rienecker, M., Schubert, S.
420 D., Sienkiewicz, M., & Zhao, B. (2017). The Modern-Era Retrospective Analysis for Research
421 and Applications, Version 2 (MERRA-2), *Journal of Climate*, 30(14), 5419-5454,
422 <https://doi.org/10.1175/JCLI-D-16-0758.1>.

423

424 Gimeno, L., Algarra, I., Eiras-Barca, J., Ramos, A. M., & Nieto, R. (2021). Atmospheric river, a
425 term encompassing different meteorological patterns. *Wiley Interdisciplinary Reviews: Water*,
426 8(6), e1558.

427

428 Global Modeling and Assimilation Office (GMAO) (2015a), MERRA-2 tavgM_2d_slv_Nx:
429 2d,Monthly mean,Time-Averaged,Single-Level,Assimilation,Single-Level Diagnostics V5.12.4,
430 Greenbelt, MD, USA, Goddard Earth Sciences Data and Information Services Center (GES
431 DISC), <https://doi.org/10.5067/AP1B0BA5PD2K>.

432

433 Global Modeling and Assimilation Office (GMAO) (2015b), MERRA-2 tavgM_2d_ocn_Nx:
434 2d,Monthly mean,Time-Averaged,Single-Level,Assimilation,Ocean Surface Diagnostics

435 V5.12.4, Greenbelt, MD, USA, Goddard Earth Sciences Data and Information Services Center
436 (GES DISC), <https://doi.org/10.5067/4IASLIDL8EEC>.

437

438 Global Modeling and Assimilation Office (GMAO) (2015c), MERRA-2 tavg1_2d_flux_Nx: 2d,1-
439 Hourly,Time-Averaged,Single-Level,Assimilation,Surface Flux Diagnostics V5.12.4, Greenbelt,
440 MD, USA, Goddard Earth Sciences Data and Information Services Center (GES DISC),
441 <https://doi.org/10.5067/7MCPBJ41Y0K6>.

442

443 Global Modeling and Assimilation Office (GMAO) (2015d), MERRA-2 inst3_3d_asm_Np:
444 3d,3-Hourly,Instantaneous,Pressure-Level,Assimilation,Assimilated Meteorological Fields
445 V5.12.4, Greenbelt, MD, USA, Goddard Earth Sciences Data and Information Services Center
446 (GES DISC), <https://doi.org/10.5067/QBZ6MG944HW0>.

447

448 Gorodetskaya, I. V., Silva, T., Schmithüsen, H., & Hirasawa, N. (2020). Atmospheric river
449 signatures in radiosonde profiles and reanalyses at the Dronning Maud Land Coast, East
450 Antarctica. *Advances in Atmospheric Sciences*, 37(5), 455–476. [https://doi.org/10.1007/s00376-](https://doi.org/10.1007/s00376-020-9221-8)
451 [020-9221-8](https://doi.org/10.1007/s00376-020-9221-8)

452

453 Gorodetskaya, I. V., Tsukernik, M., Claes, K., Ralph, M. F., Neff, W. D., & Van Lipzig, N. P.
454 M. (2014). The role of atmospheric rivers in anomalous snow accumulation in East Antarctica.
455 *Geophysical Research Letters*, 41(17), 6199–6206. <https://doi.org/10.1002/2014GL060881>

456

457 Gorodetskaya, I. V., Van Lipzig, N. P. M., Van den Broeke, M. R., Mangold, A., Boot, W., &
458 Reijmer, C. H. (2013). Meteorological regimes and accumulation patterns at Utsteinen, Dronning

459 Maud Land, East Antarctica: Analysis of two contrasting years. *Journal of Geophysical*
460 *Research: Atmospheres*, 118(4), 1700–1715. <https://doi.org/10.1002/jgrd.50177>
461

462 Gossart, A., Helsen, S., Lenaerts, J. T. M., Broucke, S. V., van Lipzig, N. P. M., & Souverijns,
463 N. (2019). An Evaluation of Surface Climatology in State-of-the-Art Reanalyses over the
464 Antarctic Ice Sheet, *Journal of Climate*, 32(20), 6899-6915, [https://doi.org/10.1175/JCLI-D-19-](https://doi.org/10.1175/JCLI-D-19-0030.1)
465 [0030.1](https://doi.org/10.1175/JCLI-D-19-0030.1).
466

467 Gutiérrez, J.M., R.G. Jones, G.T. Narisma, L.M. Alves, M. Amjad, I.V. Gorodetskaya, M. Grose,
468 N.A.B. Klutse, S. Krakovska, J. Li, D. Martínez-Castro, L.O. Mearns, S.H. Mernild, T. Ngo-
469 Duc, B. van den Hurk, and J.-H. Yoon, (2021). Atlas. In *Climate Change 2021: The Physical*
470 *Science Basis. Contribution of Working Group I to the Sixth Assessment Report of the*
471 *Intergovernmental Panel on Climate Change* [Masson-Delmotte, V., P. Zhai, A. Pirani, S.L.
472 Connors, C. Péan, S. Berger, N. Caud, Y. Chen, L. Goldfarb, M.I. Gomis, M. Huang, K. Leitzell,
473 E. Lonnoy, J.B.R. Matthews, T.K. Maycock, T. Waterfield, O. Yelekçi, R. Yu, and B. Zhou
474 (eds.)]. *Cambridge University Press*, Cambridge, United Kingdom and New York, NY, USA, pp.
475 1927–2058, doi:10.1017/9781009157896.021.
476

477 Hersbach, H., Bell, B., Berrisford, P., Hirahara, S., Horányi, A., Muñoz-Sabater, J., et al. (2020).
478 The ERA5 global reanalysis. *Quarterly Journal of the Royal Meteorological Society*, 146, 1999–
479 2049, <https://doi.org/10.1002/qj.3803>.
480

481 Korty, R. L., Camargo, S. J., & Galewsky, J. (2012). Variations in Tropical Cyclone Genesis
482 Factors in Simulations of the Holocene Epoch, *Journal of Climate*, 25(23), 8196-8211.

483

484 Lee, H.-J.; Jin, E.-K., (2021). Seasonality and Dynamics of Atmospheric Teleconnection from the
485 Tropical Indian Ocean and the Western Pacific to West Antarctica, *Atmosphere*, 12, 849.
486 <https://doi.org/10.3390/atmos12070849>.

487

488 Lenaerts, J. T. M., Ligtenberg, S. R., Medley, B., Van De Berg, W. J., Konrad, H., Nicolas, J. P.,
489 et al. (2018). Climate and surface mass balance of coastal West Antarctica resolved by regional
490 climate modelling. *Annals of Glaciology*, 59(76pt1), 29–41. <https://doi.org/10.1017/aog.2017.42>

491

492 Li, X., Gerber, E. P., Holland, D. M., & Yoo, C. (2015). A Rossby Wave Bridge from the
493 Tropical Atlantic to West Antarctica, *Journal of Climate*, 28(6), 2256-2273.
494 <https://doi.org/10.1175/JCLI-D-14-00450.1>

495

496 Lou, J., O’Kane, T.J. & Holbrook, N.J. (2021). Linking the atmospheric Pacific-South American
497 mode with oceanic variability and predictability. *Commun Earth Environ* 2, 223 (2021).
498 <https://doi.org/10.1038/s43247-021-00295-4>

499

500 Maclennan, M. L., & Lenaerts, J. T. (2021). Large-Scale Atmospheric Drivers of Snowfall Over
501 Thwaites Glacier, Antarctica. *Geophysical Research Letters*, 48 (17), e2021GL093644. doi:
502 10.1029/2021GL093644

503

504 Marshall, G. J., and Thompson, D. W. J. (2016), The signatures of large-scale patterns of
505 atmospheric variability in Antarctic surface temperatures, *J. Geophys. Res. Atmos.*, 121, 3276–
506 3289, doi:10.1002/2015JD024665.

507

508 Marshall, G.J., Thompson, D.W. and van den Broeke, M.R., (2017). The signature of Southern
509 Hemisphere atmospheric circulation patterns in Antarctic precipitation. *Geophysical Research*
510 *Letters*, 44(22), pp.11-580.

511

512 Mattingly, K. S., T. L. Mote, and Xavier Fettweis. "Atmospheric river impacts on Greenland Ice
513 Sheet surface mass balance." *Journal of Geophysical Research: Atmospheres* 123.16 (2018):
514 8538-8560.

515

516 Nuncio, M., & Yuan, X. (2015). The Influence of the Indian Ocean Dipole on Antarctic Sea Ice,
517 *Journal of Climate*, 28(7), 2682-2690. Retrieved Mar 17, 2022, from
518 <https://journals.ametsoc.org/view/journals/clim/28/7/jcli-d-14-00390.1.xml>

519

520 O'Brien, Travis Allen and Wehner, Michael F and Payne, Ashley E. and Shields, Christine A
521 and Rutz, Jonathan J. and Leung, L. Ruby and Ralph, F. Martin and Marquardt Collow, Allison
522 B. and Guan, Bin and Lora, Juan Manuel and et al., (2021). Increases in Future AR Count and
523 Size: Overview of the ARTMIP Tier 2 CMIP5/6 Experiment. *Journal of Geophysical Research-*
524 *Atmospheres*, <https://agupubs.onlinelibrary.wiley.com/doi/10.1029/2021JD036013>

525

526 Phillips, A. S., C. Deser, and J. Fasullo, (2014). A New Tool for Evaluating Modes of Variability
527 in Climate Models. *EOS*, 95, 453-455, doi: 10.1002/2014EO490002.

528

529 Pohl, B., Favier, V., Wille, J., Udy, D. G, Vance, T. R, Pergaud, J., et al. (2021). Relationship
530 between weather regimes and atmospheric rivers in East Antarctica. *Journal of Geophysical*
531 *Research: Atmospheres*, 126, e2021JD035294. <https://doi.org/10.1029/2021JD035294>

532 Power, S., Lengaigne, M., Capotondi, A., Khodri, M., Vialard, J., Jebri, B., Guilyardi, E.,
533 McGregor, S., Kug, J.S., Newman, M. and McPhaden, M.J., 2021. Decadal climate variability in
534 the tropical Pacific: Characteristics, causes, predictability, and prospects. *Science*, 374(6563),
535 p.eaay9165.

536

537 Ralph, F. M., Dettinger, M. D., Cairns, M. M., Galarneau, T. J., & Eylander, J. (2018). Defining
538 “Atmospheric River”: How the Glossary of Meteorology Helped Resolve a Debate, *Bulletin of*
539 *the American Meteorological Society*, 99(4), 837-839.

540

541 Raphael, M. N., Marshall, G. J., Turner, J., Fogt, R. L., Schneider, D., Dixon, D. A., Hosking, J.
542 S., Jones, J. M., & Hobbs, W. R. (2016). The Amundsen Sea Low: Variability, Change, and
543 Impact on Antarctic Climate, *Bulletin of the American Meteorological Society*, 97(1), 111-121.
544 <https://journals.ametsoc.org/view/journals/bams/97/1/bams-d-14-00018.1.xml>

545

546 Rutz, J.J, Shields, C.A., Lora, J.M, Payne, A.E., Guan, B., Ullrich, P., O'Brien, T., Leung, L.-Y.,
547 Ralph, F.M., Wehner, M., Brands, S., Collow, A., Goldenson, N., Gorodetskaya, I., Griffith, H.,
548 Hagos, S., Kashinath, K., Kawzenuk, B., Krishnan, H., Kurlin, V., Lavers, D., Magnusdottir, G.,

549 Mahoney, K., McClenny, E., Muszynski, G., Nguyen, P.D., Prabhat, Qian, Y., Ramos, A.M.,
550 Sarangi, C., Sellars, S., Shulgina, T., Tome, R., Waliser, D., Walton, D., Wick, G., Wilson, A.,
551 Viale, M., (2019), The Atmospheric River Tracking Method Intercomparison Project (ARTMIP):
552 Quantifying Uncertainties in Atmospheric River Climatology, *Journal of Geophysical Research-*
553 *Atmospheres* , <https://doi.org/10.1029/2019JD030936>.

554

555 Shields, C.A., J.J. Rutz, L.R. Leung, F.M. Ralph, M. Wehner, T. O'Brien, and R. Pierce, (2019).
556 Defining Uncertainties Through Comparison of Atmospheric River Tracking Methods. *Bull.*
557 *Amer. Meteor. Soc.*, 0, <https://doi.org/10.1175/BAMS-D-18-0200.1> .

558

559 Shields, C. A., Rutz, J. J., Leung, L.-Y., Ralph, F. M., Wehner, M., Kawzenuk, B., Lora, J. M.,
560 McClenny, E., Osborne, T., Payne, A. E., Ullrich, P., Gershunov, A., Goldenson, N., Guan, B.,
561 Qian, Y., Ramos, A. M., Sarangi, C., Sellars, S., Gorodetskaya, I., Kashinath, K., Kurlin, V.,
562 Mahoney, K., Muszynski, G., Pierce, R., Subramanian, A. C., Tome, R., Waliser, D., Walton, D.,
563 Wick, G., Wilson, A., Lavers, D., Prabhat, Collow, A., Krishnan, H., Magnusdottir, G., and
564 Nguyen, P. (2018), Atmospheric River Tracking Method Intercomparison Project (ARTMIP):
565 project goals and experimental design, *Geosci. Model Dev.*, 11, 2455-2474,
566 <https://doi.org/10.5194/gmd-11-2455-2018>, 2018.

567

568 Spensberger, C., Reeder, M. J., Spengler, T., & Patterson, M. (2020). The Connection between
569 the Southern Annular Mode and a Feature-Based Perspective on Southern Hemisphere
570 Midlatitude Winter Variability. *Journal of Climate*, 33(1), 115–129.

571 <https://doi.org/10.1175/JCLI-D-19-0224.1>

572

573 Terpstra, A., Gorodetskaya, I. V., & Sodemann, H. (2021). Linking sub-tropical evaporation and
574 extreme precipitation over East Antarctica: An atmospheric river case study. *Journal of*
575 *Geophysical Research: Atmospheres*, 126, e2020JD033617.

576 <https://doi.org/10.1029/2020JD033617>

577

578 Turner, J., Phillips, T., Hosking, J. S., Marshall, G. J., & Orr, A. (2013). The Amundsen Sea low.
579 *International Journal of Climatology*, 33(7), 1818–1829. <https://doi.org/10.1002/joc.3558>

580

581 Turner, J, Marshall, GJ, Clem, K, Colwell, S, Phillips, T, Lu, H. (2019). Antarctic temperature
582 variability and change from station data. *Int J Climatol*, 40: 2986– 3007.

583 <https://doi.org/10.1002/joc.6378>.

584

585 Turner, J. et al. (2019). The dominant role of extreme precipitation events in Antarctic snowfall
586 variability. *Geophys. Res. Lett.* 46, 3502–3511.

587

588 Turner, J., Lu, H., King, J. C., Carpentier, S., Lazzara, M., Phillips, T., & Wille, J. (2022). An
589 extreme high temperature event in coastal East Antarctica associated with an atmospheric river
590 and record summer downslope winds. *Geophysical Research Letters*, 49, e2021GL097108.

591 <https://doi.org/10.1029/2021GL097108>.

592

593 Wille, J.D., Favier, V., Dufour, A. et al. 2019). West Antarctic surface melt triggered by
594 atmospheric rivers. *Nat. Geosci.* 12, 911–916. <https://doi.org/10.1038/s41561-019-0460-1>

595
596 Wille, J. D., Favier, V., Gorodetskaya, I. V., Agosta, C., Kittel, C., Beeman, J. C., et al. (2021).
597 Antarctic atmospheric river climatology and precipitation impacts. *Journal of Geophysical*
598 *Research: Atmospheres*, 126, e2020JD033788. <https://doi.org/10.1029/2020JD033788>.
599
600 Wille, J.D., Favier, V., Jourdain, N., et al. , (2022), The Atmospheric River Threat to Antarctic
601 Peninsula Ice-Shelf Stability, 03 September 2021, PREPRINT (Version 1) available at Research
602 Square [<https://doi.org/10.21203/rs.3.rs-828007/v1>]
603
604 Yan, Q., Wei, T., Korty, R.L., Kossin, J.P., Zhang, Z. and Wang, H., (2016). Enhanced intensity of
605 global tropical cyclones during the mid-Pliocene warm period. *Proceedings of the National Academy of*
606 *Sciences*, 113(46), pp.12963-12967.
607
608